

ORIGINAL ARTICLE

Spin-manipulated nanoscopy for single nitrogen-vacancy center localizations in nanodiamonds

Martina Barbiero¹, Stefania Castelletto², Xiaosong Gan³ and Min Gu¹

Due to their exceptional optical and magnetic properties, negatively charged nitrogen-vacancy (NV^-) centers in nanodiamonds (NDs) have been identified as an indispensable tool for imaging, sensing and quantum bit manipulation. The investigation of the emission behaviors of single NV^- centers at the nanoscale is of paramount importance and underpins their use in applications ranging from quantum computation to super-resolution imaging. Here, we report on a spin-manipulated nanoscopy method for nanoscale resolutions of the collectively blinking NV^- centers confined within the diffraction-limited region. Using wide-field localization microscopy combined with nanoscale spin manipulation and the assistance of a microwave source tuned to the optically detected magnetic resonance (ODMR) frequency, we discovered that two collectively blinking NV^- centers can be resolved. Furthermore, when the collective emitters possess the same ground state spin transition frequency, the proposed method allows the resolving of each single NV^- center via an external magnetic field used to split the resonant dips. In spin manipulation, the three-level blinking dynamics provide the means to resolve two NV^- centers separated by distances of 23 nm. The method presented here offers a new platform for studying and imaging spin-related quantum interactions at the nanoscale with super-resolution techniques.

Light: Science & Applications (2017) 6, e17085; doi:10.1038/lsa.2017.85; published online 3 November 2017

Keywords: nanodiamonds; nanoscale microscopy; nitrogen-vacancy color centers; optically detected magnetic resonance

INTRODUCTION

Negatively charged nitrogen-vacancy (NV^-) centers in nanodiamonds (NDs) have emerged as promising fluorescent biomarkers with optical imaging and sensing applications^{1–6}. In particular, the spin transition dependent luminescence, that is, optically detected magnetic resonance (ODMR) of a single NV^- center at room temperature^{1–3,7}, provides an indispensable tool for nanoscale spin manipulation, qubit control and read out, as well as magnetic sensing in nanodiamonds^{8–14}. As such, imaging and localization of single NV^- centers are prerequisites for the subsequent development of such applications. When an oxidation process is performed, the blinking phenomenon occurs^{13,15}. Observations of intermittent photoluminescence (PL) have been reported in NV^- centers down to 5 nm discrete NDs at room temperature¹³. A qualitative explanation of the blinking PL activation based on single emitters has been given in terms of the electron tunneling processes^{13,15–18}. The blinking phenomenon and the associated non-bleaching property of NDs have enabled the super-resolution of single NV^- centers within NDs at a sub-20 nanometer resolution¹⁴.

In this work, we report on a microscopy method called spin-manipulated nanoscopy for the super-resolution imaging of multiple blinking NV^- centers, even in the presence of collective blinking. Collective blinking has been observed before at the nanoscale in

clusters of quantum dots¹⁹, and recently, multiple NV^- centers with cooperative light emissions have been observed in nanodiamonds^{20,21}.

Collective blinking phenomenon occurs when a number of identical quantum emitters are confined in a volume of $V < \lambda^3$, where λ is the wavelength of the optical transition²². Due to the spatial confinement, the emitters are indistinguishable and couple to the same emission mode and each other via resonance interactions. The smaller the confined volume of the emitters, the greater the possibility that these emitters blink collectively. Here, we observed that the fluorescences of two NV^- centers often appear to be coupled to each other, exhibiting a stochastic collective emitting behavior within the diffraction-limited region. A Monte-Carlo simulation of the stochastic collective emitting showing two NV^- centers in the 'on' state simultaneously is depicted in Figure 1a. Only one distinguishable higher fluorescence level is observed, and this impacts the resolution of the localization microscopy, which cannot distinguish between two events with cooperative fluorescence emission properties²³. Given microwave excitation resonant with an ODMR frequency, it is possible to partially suppress the cooperative emissions of the blinkers; as the transition $m_s = 0 \rightarrow m_s = \pm 1$ is induced at the on-resonant NV^- center, two distinguishable higher fluorescence levels are observed in the blinking time trace. The higher level corresponds to the two NV^- centers being in the photoluminescent 'on' state. The middle fluorescence intensity

¹Laboratory of Artificial-Intelligence Nanophotonics, School of Science, RMIT University, Melbourne, Victoria 3001, Australia; ²School of Engineering, RMIT University, Melbourne, Victoria 3000, Australia and ³Center for Micro-Photonics, Faculty of Science, Engineering and Technology, Swinburne University of Technology, PO Box 218, Hawthorn, Victoria 3122, Australia

Correspondence: M Gu, Email: Min.gu@rmit.edu.au

Received 2 January 2017; revised 8 May 2017; accepted 8 May 2017; accepted article preview online 10 May 2017

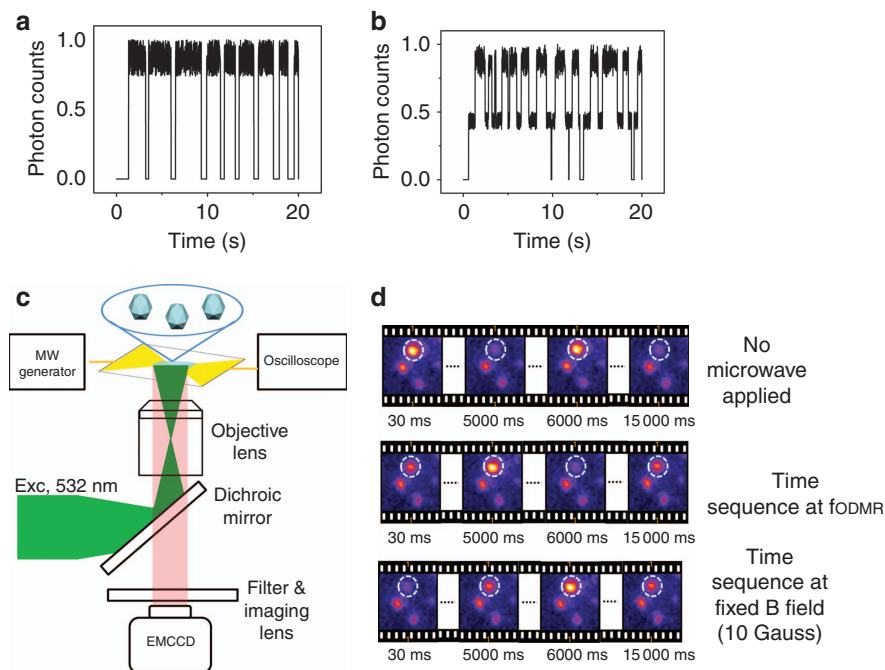


Figure 1 Dynamics of the spin-manipulated blinking fluorescence. (a) Monte-Carlo simulation of the two collectively blinking NV^- centers. Fluorescence dynamics for the two collectively blinking NV^- centers within a given ND that simultaneously blink between the 'on' and 'off' states. (b) A Monte-Carlo simulation of the stochastic blinking emission of two NV^- centers. The trace shows three different intensity levels. (c) Schematic of the wide-field setup for the spin-manipulated nanoscopy. (d) Upper: wide-field images of the NDs. The blinking ND (in the dashed circle) shows two distinctive fluorescence intensity levels; Middle: spin-manipulated nanoscopy. Each image frame is acquired at the ODMR frequency; the exposure time is 30 ms. The blinking ND (in the dashed circle) exhibits three distinctive fluorescence intensity levels; Lower: spin-manipulated nanoscopy for NV^- centers with overlapping ODMR frequencies. An external magnetic field of 10 Gauss is applied to split the ODMR dips; the exposition time is 30 ms. Similarly, the blinking ND (in the dashed circle) also exhibits three distinctive fluorescence intensity levels.

level corresponds to one emitter in the 'on' state while the other emitter is in the 'off' state and *vice versa*. The partial suppression of the collective blinking using microwave excitation is understood, assuming that only the radiative transitions from the excited state to the ground state spin sublevels contribute to the collective emissions. The non-radiative transitions to the inter-system levels, crossing from the $m_s = \pm 1$ spin states²⁴, which increase during the resonant microwave stimulation, are not collective in nature. Additionally, the $m_s = \pm 1$ spin transitions introduce dephasing in the collective emission modes coupled with the ND resonant mode²¹. The analysis of the frames with one emitting NV^- center allows the localization of the individuals²³, as confirmed by the Monte-Carlo simulation of the stochastic emitting from two NV^- centers (Figure 1b). With spin-manipulated localization microscopy, we resolve, with a nanometric resolution, the collectively blinking NV^- centers because each emitter exhibits a spin-dependent fluorescence.

MATERIALS AND METHODS

Oxidation process

A suspension of high pressure high temperature NDs with an average size of 70 nm¹⁴, which are acid cleaned and diluted in a MilliQ solution, is used. A 20-min sonication procedure is implemented to deagglomerate the NDs. A 20- μl ND solution (1:200 diluted in MilliQ water) is drop cast on an oxygen asher plasma cleaned borosilicate coverslip and dried in air. Oxidation at 450 °C for 2 h and at 600 °C for 20 min in a high temperature furnace is implemented to increase the number of blinking NDs by removing the superficial carbon atom layer of the diamond nanoparticles, eventually leaving the NV^-

emitters close to the surfaces of the NDs. When the NV^- site is close to the borosilicate coverslip, photoexcited electron(s) tunnel from the surface-proximal NV^- site to the electro-acceptor(s) located in the adjacent medium, promoting the blinking phenomenon¹⁵.

Experimental procedures

A linearly polarized beam with a wavelength of 532 nm is used as the excitation source through a 1.4 NA oil immersion objective lens. The experiment is focused around the combination of a home-built confocal microscope to measure the number of the emitters using the Hanbury Brown and Twiss (HBT) test and a wide-field microscope for the spin-manipulated nanoscopy. In the confocal configuration, the PL is coupled to two separate single-photon avalanche diodes (SPADs) via a fiber beam splitter to measure the correlation of the data with a time correlated single-photon counting card and an HBT setup. In the wide-field configuration, a flip mounted lens directs the illumination light to the back aperture of the objective lens. The same objective lens collects the emitted fluorescent light and directs it to a cooled EMCCD camera (Andor, iXon X3 897, SciTech Pty Ltd., Preston, VIC, Australia, Andor Technology Ltd., Belfast, UK) at -80 °C via a flip mounted dichroic mirror. The experimental setup for the spin-manipulated nanoscopy is schematically depicted in Figure 1c. First, the time-sequential photoluminescence images of the blinking NDs are acquired (Figure 1d, upper). Furthermore, the microwave (mw) signals for the ODMR are established using a conductive pattern imprinted on the coverslip, as reported²⁵. To measure the ODMR peak, each image frame is synchronized to a mw pulse generated from a signal generator, and the dwell time of each

mw pulse matches the exposition time of the EMCCD camera. The signal generator is also used to initialize the frame acquisitions by triggering the exposure sequence of the EMCCD camera. We captured 500 images at microwave frequencies from 2.6 to 3.0 GHz with an increment of 0.8 MHz²⁶. An ODMR frequency is identified by integrating the fluorescence of a 5×5 pixel area from the EMCCD camera. Once the ODMR frequency is determined, spin-manipulated nanoscopy can be implemented by continuously acquiring the blinking intensity of the system while the signal generator provides the mw stimulation at that ODMR frequency (Figure 1d, middle). If the ODMR resonant frequencies overlap, a uniform 10 G external magnetic field is applied to split the dips (Figure 1d, lower).

Particle detection, localization and visualization

At the ODMR frequency a total of 500 blinking cycles are recorded without bleaching. A threshold is set and a new image stack with only the frames with one emitting NV⁻ center is built, the number of blinking cycles recorded is more than 200. QuickPALM algorithm is implemented to measure the position of each NV⁻ center detected using Gaussian fitting^{27,28}. To correct the drift, one immobilized emitter is selected in the image as a reference point²³. Finally, the images are resized with the software ImageJ (US National Institutes of Health, Bethesda, MD, USA) by using an integer scale factor equal to 4 and a bilinear interpolation.

RESULTS AND DISCUSSION

Collectively blinking NDs

During collective blinking, the NV⁻ centers within the diffraction-limited region cannot be optically resolved, although the total number of emitters is discernible using autocorrelation. Without losing the generality, for the collectively blinking ND in Figure 2a, we report the HBT measurement^{29,30}. The second-order autocorrelation function $g^2(0) = 0.5$ indicates two NV⁻ centers within the diffraction-limited region. The coupling between the adjacent NV⁻ centers reveals a collective fluorescence emission with an 'on' 'off' blinking trajectory in time, and the photon count distribution (Figure 2b) shows two well separated peaks describing the 'on' and the 'off' events for the two emitters, respectively.

Effect of the oxidation process

The collective fluorescence emission is observed after the size of the NDs is reduced via oxidation (Supplementary Fig. S1). The ND dimension achieved after oxidation justifies a collective radiative emission of multiple NV⁻ centers as the NV⁻ zero-phonon line is 637 nm. As result of the reduction in size of the NDs, a decreased number of NV⁻ centers are observed (Supplementary Fig. S2a

and S2b). Moreover, the close confinement of the NV⁻ centers within the host ND increases the possibility that these emitters will blink collectively. Microwave applications combined with optical stimulations enable the detection of the ODMR resonance transitions within the oxidized ND (Supplementary Fig. S2c). At the ODMR frequency, the distribution of the photon counts clearly shows a fluorescence intermittence, confirming the blinking phenomenon (Supplementary Fig. S2d). Among all of the observed NDs after oxidation, spin-manipulated nanoscopy is applied to a single NV⁻ center in a single ND for the super-resolved spin imaging^{9,31}, and on two collectively blinking NV⁻ centers in a single ND, to resolve each single emitter.

Spin-manipulated nanoscopy of a single NV⁻ center

The second-order autocorrelation function $g^2(0) < 0.5$ and the ODMR measurement for a single NV⁻ center in an oxidized ND are reported in Figure 3a. When the resonant microwave f_1 induces the transition from $m_s = 0$ to $m_s = \pm 1$, a low photon count rate is recorded during the 'on' state of the acquired PL blinking (Figure 3b). The stochastic blinking associated with the ODMR frequency f_1 enables the assignment of spin information to the nanoscale localization. A super-resolved image of a single NV⁻ center, with a full width at half-maximum (FWHM) of 34 nm embedded within a single ND, is reconstructed (Figure 3c). When an external B field of 10 Gauss is applied, the ODMR signal shows two dips (Figure 3d). Spin-manipulated nanoscopy applied at frequencies f_2 and f_3 allows potential super-resolution imaging and parallel read outs of the NV⁻ magnetic sensitive spin. Figure 3d shows the super-resolved image of the spin state $m_s = -1$ associated with the frequency f_2 as well as the super-resolved image of the spin state $m_s = \pm 1$ associated with the frequency f_3 . The FWHM is 34 nm in both cases.

A time study of collectively blinking NDs

When an ND contains two collectively blinking NV⁻ centers, spin-manipulated nanoscopy can be implemented to partially suppress the cooperative emissions and thus the coupling between the emitters. A three-level time dependent fluorescence with distinguishable 'on' and 'off' intensity states is observed. To demonstrate that ODMR changes the blinking interactions between the NV⁻ emitters, an 'on' time duration study is carried out. To calculate the 'on' time duration, a threshold is set. In the case of collective blinking, the threshold corresponds to the background intensity value (threshold $\tau = 2000$ photon counts, Supplementary Fig. S3a, top). The 'on' time duration is calculated from the fluorescence intensity values above the threshold, which represent the collective 'on' 'on' state at the NV⁻ centers. When an ODMR frequency is applied, the threshold is above the maximum recorded 'on' 'off' fluorescence intensity (threshold $\tau = 2400$ photon

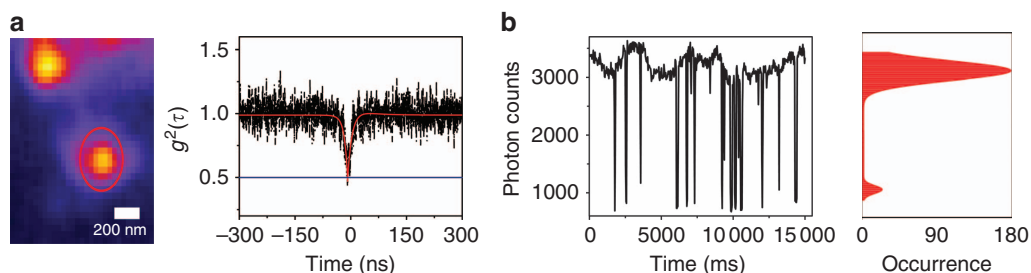


Figure 2 Collective blinking study. (a) Fluorescence image of NDs; the collectively blinking ND is in the red circle. The HBT test was performed to measure the number of emitters for the ND in the red circle. The result describes two NV⁻ centers within the ND cluster. (b) The PL intensity 'on' and 'off' trajectories and photon count distributions for the collectively blinking ND.

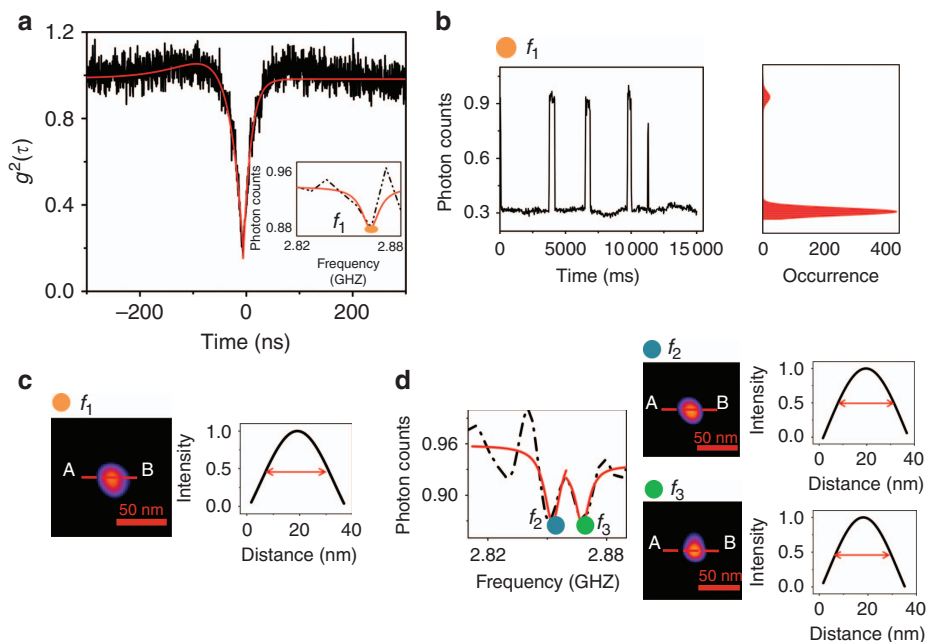


Figure 3 Spin-manipulated nanoscopy of a single NV^- center. (a) Second-order correlation function $g^2(t)$ of a single NV^- center after the oxidation treatment. In the inset, the ODMR signal shows one dip at the frequency f_1 after oxidation. (b) Stochastic ‘on’ and ‘off’ blinking and two state distribution of the photon counts per time bin recorded at the ODMR frequency f_1 . (c) Zoomed-in view of the super-resolved single NV^- center with a FWHM of 34 nm embedded within a single ND at the ODMR frequency f_1 . (d) The ODMR splits into two dips when an external B field of 10 Gauss is applied. Spin-manipulated nanoscopy is applied at the frequencies f_2 and f_3 . (Upper) The super-resolved image of the spin state $m_s = -1$, associated with the frequency f_2 , and (lower) the super-resolved image of the spin state $m_s = +1$, associated with the frequency f_3 . The FWHM is 34 nm.

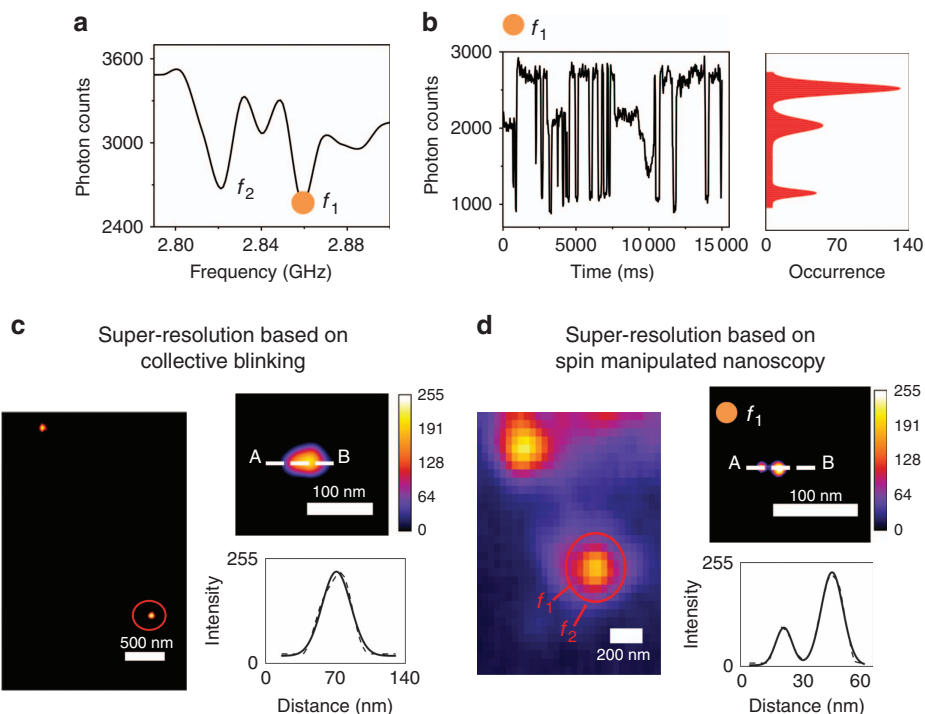


Figure 4 Spin-manipulated nanoscopy. (a) ODMR signal with two dips. (b) Blinking dynamic when fluorescence is acquired at the ODMR frequency f_1 . The photon counts per occurrence have three measured distribution states. (c) Left: super-resolution reconstructed image. The red circle highlights the collectively blinking ND. Right: (upper) zoomed-in view of the super-resolution image of the collectively blinking NV^- centers through wide-field localization microscopy; (lower) cross section showing the FWHM of 52 nm. (d) Left: fluorescence image of the collectively blinking ND. Right: (upper) zoomed-in image of the resolved NV^- centers through wide-field localization microscopy and nanoscale spin manipulation; (lower) cross section showing the 23 nm distance between the two NV^- centers.

counts, Supplementary Fig. S3a bottom)¹⁹. A histogram of the durations of the ‘on’ periods of the blinking traces represents the ‘on’ time probability distribution $P(t)_{\text{on}}$ ³². A first-order exponential-decay fitting model $P(t)_{\text{on}} \propto A_0 e^{-t/\tau_{\text{on}}}$ is performed to determine the τ_{on} durations. The fitting shows $\tau_{\text{on/on,c}} = 397.5$ ms and $\tau_{\text{on/on,i}} = 274.4$ ms. In the case of the collectively blinking NV⁻ centers, the blinking fluorescence dynamics reveal longer ‘on’ time durations ($\tau_{\text{on/on,c}}$), and this can be justified when the emitters are simultaneously in the ‘on’ state. When using spin manipulation, the emitters blink independently; therefore, they are not in the ‘on’ state simultaneously and the $(\tau_{\text{on/on,i}})$ has a shorter duration (Supplementary Fig. S3b).

Spin-manipulated nanoscopy of two collectively blinking NV⁻ centers

For the collectively blinking ND, the ODMR signal is characterized by the dips at two different frequencies, f_1 and f_2 , corresponding to two NV⁻ centers (Figure 4a). As an example, at the ODMR frequency f_1 , the spin-dependent blinking fluorescence reveals a histogram of a three-state emission configuration (Figure 4b). The higher fluorescence level corresponds to the emissions from the two NV⁻ centers, the middle fluorescence level corresponds to the emissions from only one NV⁻ center and the lower intensity level corresponds to the ‘off’ state for both NV⁻ centers. In the case of collective blinking, the super-resolution localization code can only consider the coupled fluorescence emitters with intensity distributions such that the stochastic change between an ‘on’ state and an ‘off’ state are treated as one event; thus, the centroids retrieved numerically from all of the frames are reconstructed to form a final unresolved image of one

emitter²³. Figure 4c shows the super-resolution image of the emission spot based on collective blinking; the FWHM is 52 nm. Once the spin-manipulated nanoscopy is applied, only the frames with one emitting NV⁻ center are selected during the super-resolution reconstruction process. As a result, Figure 4d shows the zoomed-in view of the resolved single NV⁻ emitters at the ODMR frequency f_1 . The reconstructed image clearly reveals two NV⁻ emitters separated by a distance of 23 nm. It is also possible to resolve the two NV⁻ emitters at the second ODMR frequency f_2 with similar results (Supplementary Fig. S4). To verify the blinking behavior of the NV⁻ centers with frequencies different from the resonant one are used, including three random frequencies f_3 , f_4 and f_5 (Supplementary Fig. S5a). At these three frequencies, the blinking trace shows collective ‘on’ and ‘off’ fluorescence emissions, and the two state photon count distributions describes the ‘on’ and the ‘off’ events for the two transmitters (Supplementary Fig. S5b–S5d). Therefore, it is the ODMR excitation that interrupts the coupling between the emitters, confirming the model of the nature of the intersystem crossing transitions in the non-cooperative emissions, and the reductions of the cooperative emissions are due mostly to the dephasing mechanism from the $m_s = \pm 1$ spin transitions²¹.

Spin-manipulated nanoscopy of two collectively blinking NV⁻ centers with overlapped ODMR frequencies

When the collective emitters possess the same ground state spin transition frequencies, an external magnetic field is applied to split the resonant dips. The collectively blinking traces and the HBT test showing two NV⁻ centers within the ND are reported in Supplementary Fig. S6. The ODMR signal shows only one dip for the two emitters (black curve in Figure 5a). When an external B field

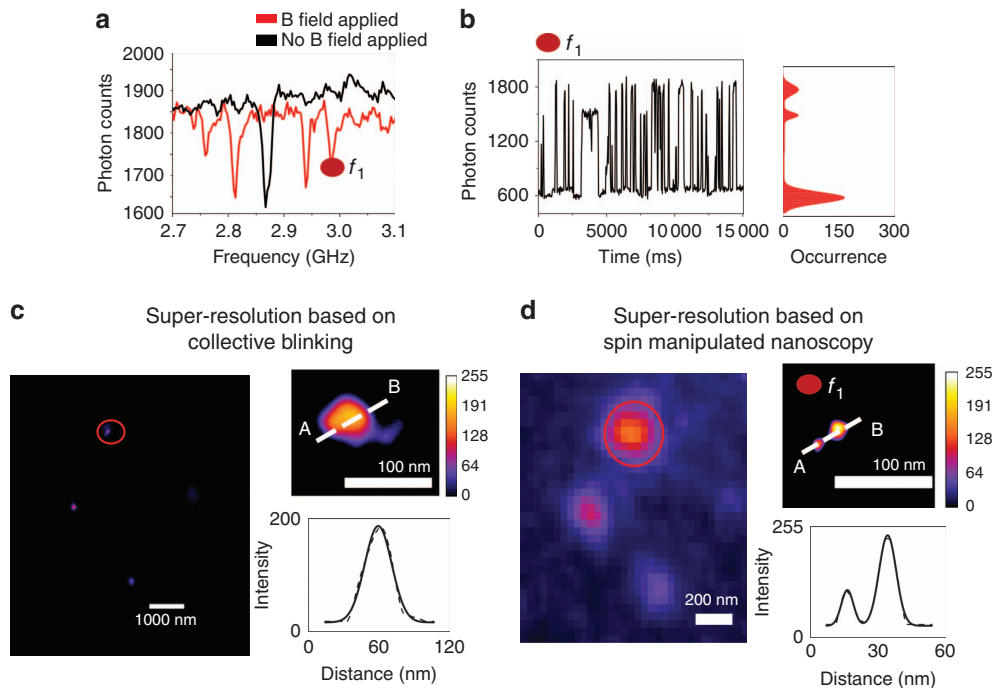


Figure 5 Spin manipulated nanoscopy with an external magnetic field. The magnetic field is applied when the collective emitters possess the same ground state spin transition frequency. (a) When an external B field of 10 Gauss is applied, the ODMR signal shows four dips (red curve). (b) Blinking fluorescence manipulated at the ODMR frequency f_1 and the photon counts per occurrence measurement, with the three distributional states. (c) Left: super-resolution reconstructed image. In the red circle, the collectively blinking ND is highlighted. Right: (upper) zoomed-in view of the super-resolution image of the collectively blinking NV⁻ centers through wide-field localization microscopy; (lower) cross section showing a FWHM of 57 nm. (d) Left: fluorescence image of the collectively blinking ND. Right: (upper) super-resolution zoomed-in image of the resolved NV⁻ centers through wide-field localization microscopy and nanoscale spin manipulation; (lower) cross section that shows the 27 nm distance between the two NV⁻ centers.

of 10 Gauss is applied, the overlapped ODMR dips, split into four dips (red curve in Figure 5a). The different shifts of the ODMR dips are caused by different factors, such as the polarization, beam power, and orientation of the magnetic field applied to the optical axis of the NV⁻ centers^{33–35}. Once spin-manipulated nanoscopy is applied at frequency f_1 (Figure 5a); the spin-dependent blinking fluorescence and photon count distribution at frequency f_1 show three states (Figure 5b). The reconstructed image based on the collective blinking data shows a single emission spot with an FWHM of 57 nm (Figure 5c). In Figure 5d the zoomed-in area of the resolved single NV⁻ centers, using the ODMR frequency f_1 . The reconstructed image reveals two NV⁻ emitters separated by 27 a distance of nm.

CONCLUSION

The combination of the spin read out and sensing with the super-resolution imaging and nanometric localization of single NV⁻ centers has been at the center of many proposed methods for advancing nanometric magnetic resonance imaging^{9,31,36–39}. In this work, we have presented spin-manipulated nanoscopy to resolve single NV⁻ centers in blinking NDs with an average size of 42 nm, where the photoluminescence intermittency is achieved via oxidation^{13–16}. The relevance of the super-resolution methods applied to the NDs is motivated by their wide range of applications in the life sciences compared to bulk diamonds⁴⁰. Furthermore, smaller probes are a common need in biomedical imaging, and the blinking phenomenon is more likely when the size of the nanodiamonds is reduced. Our method allows the imaging of the spin states at the nanoscale in individual NV⁻ centers in single blinking NDs. Each single emitter is resolved independently from its off-resonant image, which is necessary for the super-resolution technique, based on the spectral differences⁹. The proposed method enables the decoupling of the collectively blinking emissions and, thus, image reconstruction using different temporal domain frames can be utilized, as can that with different spectral domains. By manipulating the spin states of two collectively blinking NV⁻ centers, it is possible to identify the localization of single NV⁻ centers in collectively blinking nanodiamonds separated by nanometer distances under resonant microwave radiation. Further, the application of an external magnetic field enables the resolution of the collective emitters when they possess the same ground state spin transition frequency.

The potential to distinguish different color centers within the same nanodiamond enables the nanoscale reconstruction of the magnetic resonance image of closely spaced NV⁻ centers. Therefore, the presented method adds a greater value to the applications of NDs as biomarkers for super-resolved magnetic imaging in the life sciences.

CONFLICT OF INTEREST

The authors declare no conflict of interest.

AUTHOR CONTRIBUTIONS

MB and MG conceived the idea and designed the research and experiments; SC provided the nanodiamonds and XG performed the Monte-Carlo simulations. All authors were involved in the analysis of the data and discussed the manuscript.

ACKNOWLEDGEMENTS

Min Gu thanks the Australian Research Council Laureate Fellowship project (FL100100099).

- 1 Taylor JM, Cappellaro P, Childress L, Jiang L, Budker D *et al*. High-sensitivity diamond magnetometer with nanoscale resolution. *Nat Phys* 2008; **4**: 810–816.
- 2 Maze JR, Stanwix PL, Hodges JS, Hong S, Taylor JM *et al*. Nanoscale magnetic sensing with an individual electronic spin in diamond. *Nature* 2008; **455**: 644–647.
- 3 Balasubramanian G, Chan IY, Kolesov R, Al-Hmoud M, Tisler J *et al*. Nanoscale imaging magnetometry with diamond spins under ambient conditions. *Nature* 2008; **455**: 648–651.
- 4 Le Sage D, Arai K, Glenn DR, DeVience SJ, Pham LM *et al*. Optical magnetic imaging of living cells. *Nature* 2013; **496**: 486–489.
- 5 Shi FZ, Zhang Q, Wang PF, Sun HB, Wang JR *et al*. Single-protein spin resonance spectroscopy under ambient conditions. *Science* 2015; **347**: 1135–1138.
- 6 Schirhagl R, Chang K, Loretz M, Degen CL. Nitrogen-vacancy centers in diamond: nanoscale sensors for physics and biology. *Annu Rev Phys Chem* 2014; **65**: 83–105.
- 7 Steinert S, Dolde F, Neumann P, Aird A, Naydenov B *et al*. High sensitivity magnetic imaging using an array of spins in diamond. *Rev Sci Instrum* 2010; **81**: 043705.
- 8 Fedotov IV, Doronina-Amitonova LV, Voronin AA, Levchenko AO, Zibrov SA *et al*. Electron spin manipulation and readout through an optical fiber. *Sci Rep* 2014; **4**: 5362.
- 9 Chen EH, Gaathon O, Trusheim ME, Englund D. Wide-field multispectral super-resolution imaging using spin-dependent fluorescence in nanodiamonds. *Nano Lett* 2013; **13**: 2073–2077.
- 10 Holt KB. Diamond at the nanoscale: applications of diamond nanoparticles from cellular biomarkers to quantum computing. *Phil Trans R Soc A Math Phys Eng Sci* 2007; **365**: 2845–2861.
- 11 Rondin L, Tetienne JP, Hingant T, Roch JF, Maletinsky P *et al*. Magnetometry with nitrogen-vacancy defects in diamond. *Rep Prog Phys* 2014; **77**: 056503.
- 12 Castelletto S, Li X, Gu M. Frontiers in diffraction unlimited optical methods for spin manipulation, magnetic field sensing and imaging using diamond nitrogen vacancy defects. *Nanophotonics* 2012; **1**: 139–153.
- 13 Bradac C, Gaebel T, Naidoo N, Sellars MJ, Twamley J *et al*. Observation and control of blinking nitrogen-vacancy centres in discrete nanodiamonds. *Nat Nanotechnol* 2010; **5**: 345–349.
- 14 Gu M, Cao YY, Castelletto S, Kouskousis B, Li XP. Super-resolving single nitrogen vacancy centers within single nanodiamonds using a localization microscope. *Opt Express* 2013; **21**: 17639–17646.
- 15 Bradac C, Gaebel T, Pakes CI, Say JM, Zvyagin AV *et al*. Effect of the nanodiamond host on a nitrogen-vacancy color-centre emission state. *Small* 2013; **9**: 132–139.
- 16 Gaebel T, Bradac C, Chen J, Say JM, Brown L *et al*. Size-reduction of nanodiamonds via air oxidation. *Diamond Relat Mater* 2012; **21**: 28–32.
- 17 Cichos F, von Borczyskowski C, Orrit M. Power-law intermittency of single emitters. *Curr Opin Colloid Interface Sci* 2007; **12**: 272–284.
- 18 Kuno M, Fromm DP, Johnson ST, Gallagher A, Nesbitt DJ. Modeling distributed kinetics in isolated semiconductor quantum dots. *Phys Rev B* 2003; **67**: 125304.
- 19 Wang SY, Querner C, Dadosh T, Crouch CH, Novikov DS *et al*. Collective fluorescence enhancement in nanoparticle clusters. *Nat Commun* 2011; **2**: 364.
- 20 Juan ML, Bradac C, Besga B, Johnsson M, Brennen G *et al*. Cooperatively enhanced dipole forces from artificial atoms in trapped nanodiamonds. *Nat Phys* 2016; **13**: 241–245.
- 21 Bradac C, Johnsson M, van Breugel M, Baragiola B, Martin R *et al*. Observation of room-temperature spontaneous superradiance from single diamond nanocrystals. Digest Version [PDF on Internet]. Sydney: Australia [Updated 10 August 2016]. Available at: <https://arxiv.org/abs/1608.03119>.
- 22 Scheibner M, Schmidt T, Worschech L, Forchel A, Bacher G *et al*. Superradiance of quantum dots. *Nat Phys* 2007; **3**: 106–110.
- 23 Chien FC, Kuo CW, Chen PL. Localization imaging using blinking quantum dots. *Analyst* 2011; **136**: 1608–1613.
- 24 Doherty MW, Manson NB, Delaney P, Jelezko F, Wrachtrup J *et al*. The nitrogen-vacancy colour centre in diamond. *Phys Rep* 2013; **528**: 1–45.
- 25 Dolan PR, Li XP, Storteboom J, Gu M. Complete determination of the orientation of NV centers with radially polarized beams. *Opt Express* 2014; **22**: 4379–4387.
- 26 Gruber A, Dräbenstedt A, Tietz C, Fleury L, Wrachtrup J *et al*. Scanning confocal optical microscopy and magnetic resonance on single defect centers. *Science* 1997; **276**: 2012–2014.
- 27 Henriques R, Lelek M, Fornasiero EF, Valtorta F, Zimmer C *et al*. QuickPALM: 3D real-time photoactivation nanoscopy image processing in ImageJ. *Nat Methods* 2010; **7**: 339–340.
- 28 Thompson RE, Larson DR, Webb WW. Precise nanometer localization analysis for individual fluorescent probes. *Biophys J* 2002; **82**: 2775–2783.
- 29 Hanbury Brown R, Twiss RQ. A test of a new type of stellar interferometer on Sirius. *Nature* 1956; **178**: 1046–1048.
- 30 Hanbury Brown R, Twiss RQ. Correlation between photons in two coherent beams of light. *Nature* 1956; **177**: 27–29.
- 31 Pfender M, Aslam N, Waldherr G, Neumann P, Wrachtrup J. Single-spin stochastic optical reconstruction microscopy. *Proc Natl Acad Sci USA* 2014; **111**: 14669–14674.
- 32 Crouch CH, Sauter O, Wu XH, Purcell R, Querner C *et al*. Facts and artifacts in the blinking statistics of semiconductor nanocrystals. *Nano Lett* 2010; **10**: 1692–1698.
- 33 Dréau A, Lesik M, Rondin L, Spinicelli P, Arcizet O *et al*. Avoiding power broadening in optically detected magnetic resonance of single NV defects for enhanced DC-magnetic field sensitivity. *Phys Rev B* 2011; **84**: 195204.
- 34 Tetienne JP, Rondin L, Spinicelli P, Chipaux M, Debuisschert T *et al*. Magnetic-field-dependent photodynamics of single NV defects in diamond: an application to qualitative all-optical magnetic imaging. *New J Phys* 2012; **14**: 103033.

- 35 Epstein RJ, Mendoza FM, Kato YK, Awschalom DD. Anisotropic interactions of a single spin and dark-spin spectroscopy in diamond. *Nat Phys* 2005; **1**: 94–98.
- 36 Arroyo-Camejo S, Adam MP, Besbes M, Hugonin JP, Jacques V *et al*. Stimulated emission depletion microscopy resolves individual nitrogen vacancy centers in diamond nanocrystals. *ACS Nano* 2013; **7**: 10912–10919.
- 37 Chen XD, Zou CL, Gong ZJ, Dong CH, Guo GC *et al*. Subdiffraction optical manipulation of the charge state of nitrogen vacancy center in diamond. *Light Sci Appl* 2015; **4**: e230, doi:10.1038/lsa.2015.3.
- 38 Wildaner D, Maze JR, Hell SW. Diffraction unlimited all-optical recording of electron spin resonances. *Phys Rev Lett* 2011; **107**: 017601.
- 39 Maurer PC, Maze JR, Stanwix PL, Jiang L, Gorshkov AV *et al*. Far-field optical imaging and manipulation of individual spins with nanoscale resolution. *Nat Phys* 2010; **6**: 912–918.
- 40 Mochalin VN, Shenderova O, Ho D, Gogotsi Y. The properties and applications of nanodiamonds. *Nat Nanotechnol* 2012; **7**: 11–23.



This work is licensed under a Creative Commons Attribution-NonCommercial-NoDerivs 4.0 International License. The images or other third party material in this article are included in the article's Creative Commons license, unless indicated otherwise in the credit line; if the material is not included under the Creative Commons license, users will need to obtain permission from the license holder to reproduce the material. To view a copy of this license, visit <http://creativecommons.org/licenses/by-nc-nd/4.0/>

© The Author(s) 2017

Supplementary Information for this article can be found on the *Light: Science & Applications*' website (<http://www.nature.com/lsa>).